A link between microwave extinction length, firn thermal diffusivity, and accumulation rate in West Antarctica

Lora S. Koenig,[1] Eric J. Steig,[1] Dale P. Winebrenner,[1,2] and Christopher A. Shuman[3]

Received 20 October 2006; revised 9 March 2007; accepted 3 May 2007; published 16 August 2007.

[1] The relationship between time series of physical surface temperature and microwave brightness temperature of polar firn depends both on the physical properties of the firn and the surface temperature history. In perennially dry firn this relationship is well characterized by a timescale, referred to as the extinction-diffusion time, which is the ratio of the microwave extinction length squared to the firn thermal diffusivity. The extinction-diffusion time is calculated over Antarctica from 1982 to 1999 by comparing thermal infrared observations of physical surface temperature from the advanced very high resolution radiometer (AVHRR) with passive microwave brightness temperatures measured by the scanning multichannel microwave radiometer (SMMR) and Special Senor Microwave Imager (SSM/I). Independent estimates of accumulation rate are derived both from ice cores and from spatially extensive ground and airborne radar echo sounding lines. The extinction-diffusion time is found to vary linearly with accumulation rate from approximately 10 to 50 cm/yr ice equivalent over a large area in West Antarctica. Although this simple relationship does not appear to hold at very low or very high accumulation rates, these results suggest that the extinction-diffusion time holds promise as a viable proxy for accumulation rate variability on polar ice sheets.

Citation: Koenig, L. S., E. J. Steig, D. P. Winebrenner, and C. A. Shuman (2007), A link between microwave extinction length, firn thermal diffusivity, and accumulation rate in West Antarctica, *J. Geophys. Res.*, *112*, F03018, doi:10.1029/2006JF000716.

1. Introduction

[2] Polar-orbiting satellites provide the leading tool for monitoring the Antarctic and Greenland ice sheets. Satellite sensors collect spatially distributed data sets that can be used to derive temperature, surface height, surface velocity, snow properties, and melt on ice sheets [*Bindschadler*, 1998]. Snow accumulation rate measurements are of particular interest on ice sheets, both for studies of polar climate variability and for assessments of ice sheet mass balance. Ground-based measurements of accumulation from snow pits, firn cores, and automatic weather station (AWS) sites, though numerous, are sporadic in space and time [*Vaughan et al.*, 1999]. Satellite-based measurements of accumulation rate can be derived from laser altimetry data after correction for firn densification and ice dynamics. These altimetry data, although very precise, are limited by short operation time. Broad ice sheet coverage by laser altimetry with subannual resolution started in 2003 [*Shuman et al.*, 2006]. In contrast to ground-based measurements and altimetry data, space-borne passive microwave sensors provide data that are spatially and temporally extensive with operations since 1978 covering both the Greenland and Antarctic ice sheets. The length and continuity of these data give considerable motivation for developing techniques for determining accumulation from passive microwave sensors.

[3] Satellite data from passive microwave emission are well suited for polar studies in the dry snow zone. Emission at frequencies of 37 GHz and lower are unaffected by the dry polar atmosphere. As discussed in numerous texts [e.g., *Hall and Martinec*, 1985], microwave emission in firn emerges over some characteristic depth or extinction length. Typical microwave extinction lengths in perennially dry polar firn range from fractions of a meter to tens of meters, depending on frequency. The microwave emission observed from space is most sensitive to firn properties at depths less than the extinction length. The importance of the firn properties to the passive microwave signal increases nonlinearly toward the snow-air interface. Relevant firn properties include temperature, grain size, density, layering, and grain shape [*Hall*, 1987; *Matzler*, 1987; *Surdyk*, 2002; *Zwally*, 1977]. Because these same firn properties are sensitive to accumulation rate changes, it is expected that there will be some relationship between passive microwave emission and accumulation rate.

[4] Previous attempts to relate microwave emission to accumulation rate have relied on estimates of an effective emissivity or the polarization of emission from polar firn [*Vaughan et al.*, 1999; *Winebrenner et al.*, 2001; *Zwally and Giovinetto*, 1995; *Zwally*, 1977]. These efforts have suffered

[1]Department of Earth and Space Sciences, University of Washington, Seattle, Washington, USA.
[2]Applied Physics Laboratory, University of Washington, Seattle, Washington, USA.
[3]Planetary Geodynamics Branch, NASA Goddard Space Flight Center, Greenbelt, Maryland, USA.

Copyright 2007 by the American Geophysical Union.
0148-0227/07/2006JF000716

from various problems, including poor correlation with available ground-based accumulation rate data.

[5] In this paper, we revisit the relationship between accumulation rate and microwave emission using a more complete model of firn emission properties, following *Winebrenner et al.* [2004]. The model simulates passive microwave emission over dry snow regions on ice sheets by solving the radiative transfer equation, neglecting the multiple scattering term, while using surface temperatures to force the heat diffusion equation, which establishes a temperature profile in the firn and supplies the needed temperature in the radiative transfer equation. We take advantage of infrared satellite data to provide an independent estimate of the surface temperature forcing covering the entire ice sheet. The surface temperature forcings are used in the *Winebrenner et al.* [2004] model (see section 2) to simulate microwave brightness temperatures, which are compared to observed microwave brightness temperatures. Using both observed and calculated microwave brightness temperature and observed surface temperature forcing provides a means to directly calculate the ratio of the microwave extinction length squared to the firn thermal diffusivity. Spatial variations in this ratio are found to vary linearly with variations in accumulation rates over a large region of West Antarctica and over a broad range of values (10–50 cm/yr ice equivalent).

2. Background

[6] Thermal microwave emission from dry firn consists of contributions from a range of depths below the surface [*Zwally*, 1977]. Emitted intensity therefore depends on the vertical temperature profile in the ice sheet over that range as well as the firn characteristics. The vertical temperature profile is determined by past surface temperature forcing [*Paterson*, 1994]. An observation of the microwave brightness temperature at any given moment thus depends not only on the surface temperature at that moment but also on past surface temperature forcing as well as the thermal and microwave extinction properties of the firn [*Winebrenner et al.*, 2004].

[7] If surface temperature, $T(t)$, remained constant at some value, $\overline{T}$, for long enough to make the firn isothermal over the entire depth range pertinent to microwave emission, then the brightness temperature, $T_B(t)$, would also be constant in time at some value $\overline{T}_B$. $\overline{T}_B$ would then relate to the firn temperature as

$$\overline{T}_B = \varepsilon \overline{T}, \tag{1}$$

where ε is the emissivity. In equation (1) the assumption is made that the Rayleigh-Jeans approximation holds for microwave frequencies and ice sheet temperatures.

[8] Equation (1) remains valid when $\overline{T}$ and $\overline{T}_B$ are long-term means of the time-varying surface and brightness temperatures, provided that the mean of the temperature profile in the firn is constant with depth. For annual averages, equation (1) closely approximates microwave observations [*Zwally*, 1977]. On shorter timescales, *Shuman et al.* [1995], *Shuman and Stearns* [2001], *Shuman and Comiso* [2002], and *Surdyk* [2002] showed that surface and brightness temperature means over periods approximately a month or longer can be related by a modified version of equation (1):

$$\overline{T}_B(t) = \varepsilon(t)\overline{T}(t). \tag{2}$$

In equation (2), $\overline{T}(t)$ and $\overline{T}_B(t)$ are means on approximately monthly or longer timescales. The emissivity, $\varepsilon(t)$, is allowed to vary in time to account for the changing contributions to emission from various depths as the temperature profile changes during the year.

[9] Equation (2) fails to accurately approximate means over timescales shorter than the time needed for surface temperature forcing to propagate to all depths that contribute to observed emission. In fact, strictly speaking, no instantaneous relationship such as equation (2) can explain emission at time t in terms of a surface temperature at time t alone. The instantaneous relationship must fail because temperature profiles cannot respond instantaneously to changes at the surface [*Paterson*, 1994]. Rather, emission at the present time, t, must depend on the physical memory at depth of past surface temperatures and on the weighting of emission contributions from those depths. After modest simplifying assumptions, the result is a weighted sum over surface temperature forcing, or a convolution [*Winebrenner et al.*, 2004, equation 9]:

$$T_B(t) = \varepsilon\overline{T} + \varepsilon \int_0^{\frac{t}{\tau_0}} T_f(t - \tau_0\tau')G(\tau')d\tau', \tag{3}$$

where $\overline{T}$ is the long-term (annual or longer) mean of surface temperature, ε is the time invariant emissivity defined by equation (1), $T_f(t) = T(t) - \overline{T}$ is the fluctuating part of the surface temperature, G is the convolution kernel,

$$G(\tau') = \frac{1}{\sqrt{\pi\tau'}} - \exp(\tau')\mathrm{erfc}\left(\sqrt{\tau'}\right), \tag{4}$$

erfc is the complimentary error function, and τ_0 is the characteristic timescale of averaging over past surface temperature variations. Here τ_0 is referred to as the extinction-diffusion time:

$$\tau_0 = \frac{L^2}{K}, \tag{5}$$

where L is the extinction length (the depth scale of microwave extinction in the firn) and K is the thermal diffusivity of firn at depths commensurate with L.

[10] Spatial and temporal variation in the extinction-diffusion time is expected to correlate with changes in firn properties that control firn thermal diffusivity and the microwave extinction length. Thermal diffusivity is controlled by changes in thermal conductivity and density, while extinction length in dry snow is controlled by changes in grain size, layering, and density. *Courville et al.* [2007] took measurements of thermal conductivity in a "megadunes" region near Vostok, East Antarctica, and show a decrease in thermal conductivity with increased accumulation at sites with very low accumulation rates. Extinction length should also be correlated with accumulation owing to the influence of density and grain size variations [*Surdyk*, 2002]. Snow grains at lower accumulation sites sit at the

snow-air interface for longer periods of time relative to high-accumulation sites. The low-accumulation snow grains are exposed to larger temperature gradients at the snow-air interface, leading to constructive metamorphosis and hence larger snow grains. In general, extinction length will decrease as snow grain size increases; thus extinction length should increase with accumulation rate. We therefore expect the extinction-diffusion time (the ratio of extinction length squared and the thermal diffusivity) to increase with accumulation rate.

3. Data and Methods

[11] To investigate changes in the extinction-diffusion time (τ_0) over space and time, we compare simulated passive microwave data with observed passive microwave data. The simulated data are calculated using equation (3), and surface temperature time series data sets are discussed further below. The Defense Meteorological Satellite Program (DMSP) data sets from the scanning multichannel microwave radiometer (SMMR) and the Special Sensor Microwave Imager (SSM/I) provide the observed passive microwave (T_B) measurements on daily and monthly scales [*Gloerson et al.*, 1990; *Maslanik and Stroeve*, 1990]. We use T_B values from both the 18/19 and 37 GHz vertically polarized channels, abbreviated 19 V and 37 V, respectively, because they provide the longest record of consistently acquired data and are less affected by surface roughness than horizontally polarized channels. While we have chosen to use the long time series provided by the SMMR and SMM/I data sets for this work, it is noted that the Advanced Microwave Scanning Radiometer–EOS (AMSR-E) data set can work equally well.

[12] Two surface temperature (T_S) data sets were used as model inputs: near-surface (~1 m screen height) automatic weather station (AWS) data from the Antarctic AWS Project (University of Wisconsin, see http://uwamrc.ssec.wisc.edu/aws.html) and thermal infrared surface skin temperature observations from the advanced very high resolution radiometer (AVHRR) [*Comiso*, 2000]. These two complimentary data sets were used because AWS time series provide daily resolution but only at isolated points, whereas the AVHRR data provide broad spatial coverage but with reduced temperature fidelity. AWS data were used only if there were two or more consecutive years of data with no more than two consecutive missing days; the mean value of adjacent days was used to fill missing days. AVHRR temperatures provide spatially distributed T_S data on monthly timescales from 1982 to 1999 [*Comiso*, 2000]. The AVHRR data are monthly averaged because surface measurements are valid only on cloud-free days. There were no missing monthly data points, but not all months are composed of the same number of daily observations. The 5 km × 5 km AVHRR surface temperatures were resampled to the 25 km × 25 km SSM/I grid, for comparison with the microwave T_B data.

[13] To determine the extinction-diffusion time, τ_0, the surface temperature data are used to simulate passive microwave brightness temperature data for a large range of τ_0 values (see equation (3)). The τ_0 value is determined by the optimizing the fit between simulated and observed T_B. The best fit is defined as the single minimum of the squared residuals between the fractional variation in the observed and simulated T_B, following *Winebrenner et al.* [2004]. Figure 1 shows the fit curve for τ_0 (Figure 1, left) and the daily fractional variation of AWS-simulated T_B compared to the satellite observed T_B (Figure 1, right) for four representative locations over several years. Plots similar to Figure 1 can be derived for any AWS site with two or more consecutive years of data in the dry snow zone. Uncertainty in the estimate of τ_0 is calculated by adding normally distributed random noise to the satellite T_B time series with a standard deviation of 2 K, based on the SSM/I sensor sensitivity [*Hollinger et al.*, 1990]. Typical error values are ±1 day.

[14] Best fit values of τ_0 were calculated from both daily AWS and monthly mean IR T_S data. Daily averaged T_B were used to determine τ_0 in pixels with AWS stations while monthly averaged T_B were used to determine τ_0 at pixels with AVHRR data. At pixels where both AWS and AVHRR data are available, there is little discrepancy. Table 1 compares the best fit τ_0 calculated from the longest AWS time series available at representative sites to the best fit τ_0 calculated from the AVHRR data set from 1982 to 1999. Directly comparing the τ_0 calculated from AWS data and AVHRR data over simultaneous time periods is difficult because the AWS data are sporadic; however, as shown in Table 1, at most sites the AWS τ_0 are comparable to the AVHRR τ_0.

[15] Point source measurements limit accuracy when looking at spatial phenomena, like temperature and accumulation, so we use the AVHRR spatial fields to look at variations in τ_0 over space. The monthly AVHRR T_S data set was used to simulate monthly averaged T_B over all of Antarctica (equation (3)). The simulated T_B were then compared to the monthly averaged SMMR or SSM/I T_B

Figure 1. (left) Plots of the root-mean-square difference (RMSD) between simulated and observed time series of the fractional variation in brightness temperature versus the value of the extinction-diffusion timescale, τ_0, used for simulation at four automatic weather station (AWS) sites. (Fractional variation in a brightness temperature, $T_B(t)$, is defined as $[T_B(t) - \overline{T}]/\overline{T}$, where $\overline{T}$ is the long-term mean value of $T_B(t)$.) Values of τ_0 at which the RMSD is minimized are defined as the best fit values. (right) Simulated (solid lines) and observed (shaded lines) fractional variations in vertically polarized, 37 GHz brightness temperatures for Special Senor Microwave Imager (SSM/I) pixels containing the four AWS sites for the best fit value of τ_0 at that site as indicated by Figure 1 (left). Note the range in values of best fit τ_0 and the agreement between simulations and data on timescales ranging from years to a few days. The four AWS sites represent a wide variety of Antarctic conditions. (Dome C is a low-accumulation site in East Antarctica, Lynn is in a katabatic wind region near the ice sheet edge, Siple is in a high-accumulation area near the base of the Antarctic Peninsula, and Byrd is near an ice sheet divide in West Antarctica.) Locations of AWS sites are shown in Figure 2.

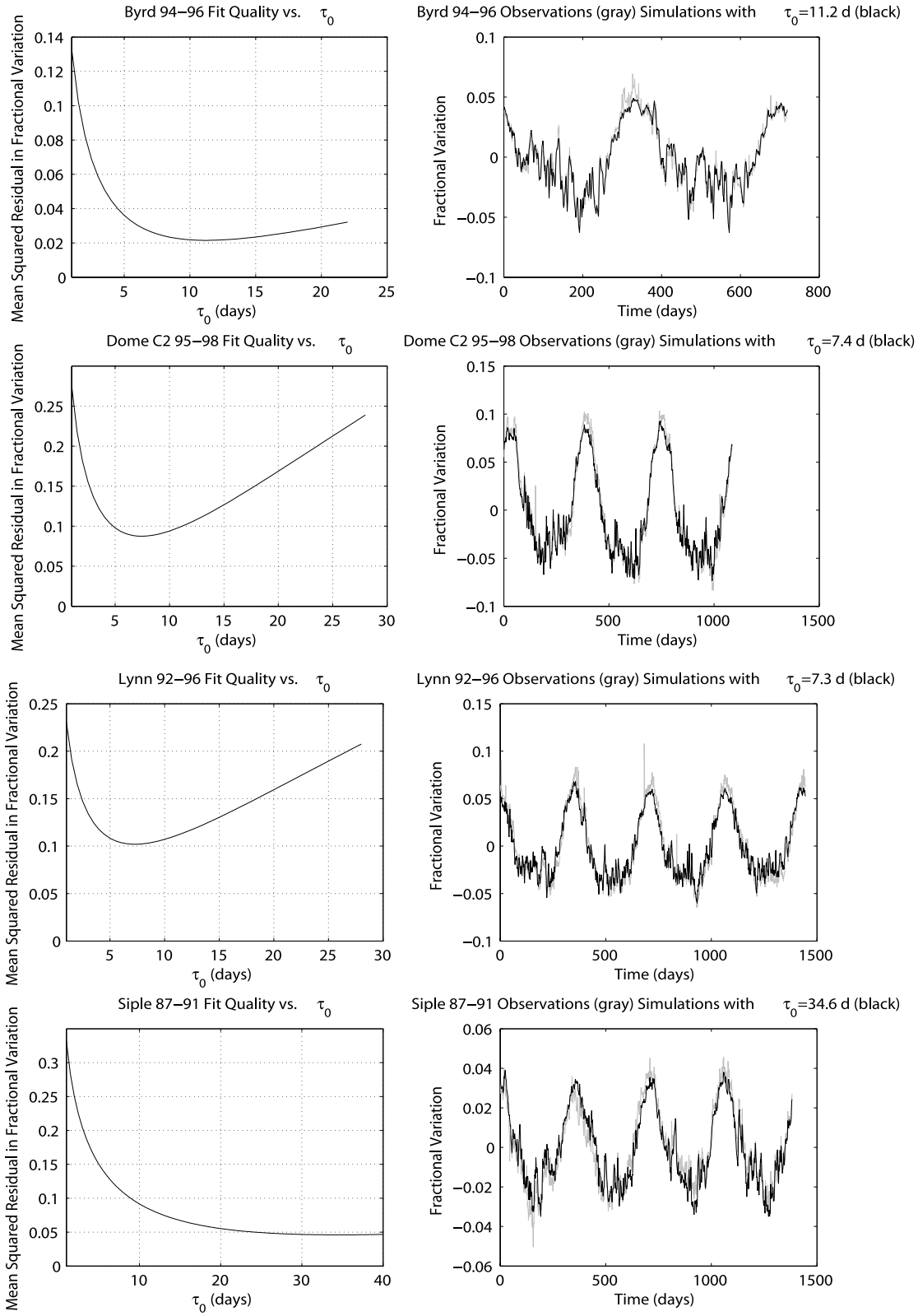
Byrd 94–96 Fit Quality vs. τ_0
Mean Squared Residual in Fractional Variation
τ_0 (days)
Byrd 94–96 Observations (gray) Simulations with τ_0=11.2 d (black)
Fractional Variation
Time (days)
Dome C2 95–98 Fit Quality vs. τ_0
Mean Squared Residual in Fractional Variation
τ_0 (days)
Dome C2 95–98 Observations (gray) Simulations with τ_0=7.4 d (black)
Fractional Variation
Time (days)
Lynn 92–96 Fit Quality vs. τ_0
Mean Squared Residual in Fractional Variation
τ_0 (days)
Lynn 92–96 Observations (gray) Simulations with τ_0=7.3 d (black)
Fractional Variation
Time (days)
Siple 87–91 Fit Quality vs. τ_0
Mean Squared Residual in Fractional Variation
τ_0 (days)
Siple 87–91 Observations (gray) Simulations with τ_0=34.6 d (black)
Fractional Variation
Time (days)

Figure 1

Table 1. Comparison of Best Fit τ_0 Derived From AWS and AVHRR Surface Temperature Data[a]

Station	AWS T_S Dates	τ_0 AWS, months	AVHRR T_S Dates	τ_0 AVHRR, months
Byrd	1981–1988	0.56	1982–1999	0.53
Dome C	1984–1995	0.51	1982–1999	0.60
Dome C II	1995–1998	0.25	1982–1999	0.31
Siple	1987–1991	1.15	1982–1999	0.88

[a]The locations of the AWS stations are shown in Figure 2. AWS, automatic weather station; AVHRR, advanced very high resolution radiometer.

data sets to best fit τ_0 over the dry snow zone of Antarctica (Figure 2).

[16] The spatial τ_0 fields were compared to accumulation measurements. We compiled accumulation data sets from ice-penetrating radar and shallow ice cores. Point source accumulation rates were derived from 14 shallow ice cores obtained by the U.S. International Trans-Antarctic Scientific Expedition (ITASE) program [*Kaspari et al.*, 2005]. A spatial grid of accumulation rates was generated from numerous ice-penetrating radar flights near Byrd Station, Antarctica [*Morse et al.*, 2002]. Accumulation rate was determined from the depth of continuous radar horizons that intersected the Byrd ice core. The radar-based accumulation rates represent an average over the past 2500 years; the depth penetrated far exceeds the expected extinction length of passive microwave sensors, but this data set is the best spatial estimate of accumulation patterns currently available. An additional accumulation data set is derived from a single ground-based radar transect between U.S. ITASE shallow ice cores [*Spikes et al.*, 2004]. The ITASE radar-based accumulation data represent an average from 1966 to 2000.

[17] Spatial variations in τ_0 and comparison to accumulation were calculated using both 19V and 37V passive microwave brightness temperatures. The results at each frequency are nearly identical, so we show only the 37 GHz results here.

4. Results/Discussion

[18] The extinction-diffusion time, τ_0, varies spatially and temporally. Figure 2 shows calculated τ_0 for Antarctica at

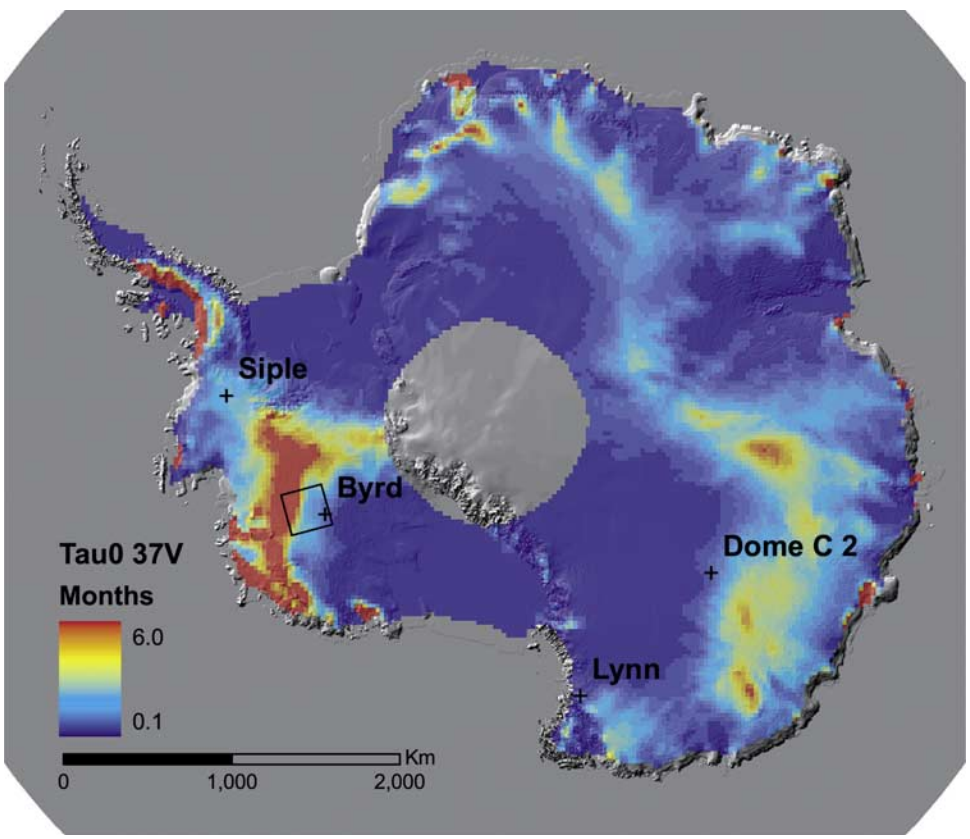

Figure 2. Spatial variability in best fit values of τ_0 on the Antarctic continent as observed using the scanning multichannel microwave radiometer (SMMR) and Special Senor Microwave Imager (SSM/I), excluding areas that melt seasonally. Here τ_0 is calculated using the entire time series from 1982 to 1999. Variability in East Antarctica appears to be associated with ice divides and does not obviously correspond with known variability in accumulation rates. Variability near the West Antarctic Divide, however, does correspond with known accumulation rate variability. The box shows the location of the radar-generated accumulation data set used in Figures 4 and 5. The crosses denote locations of AWS stations.

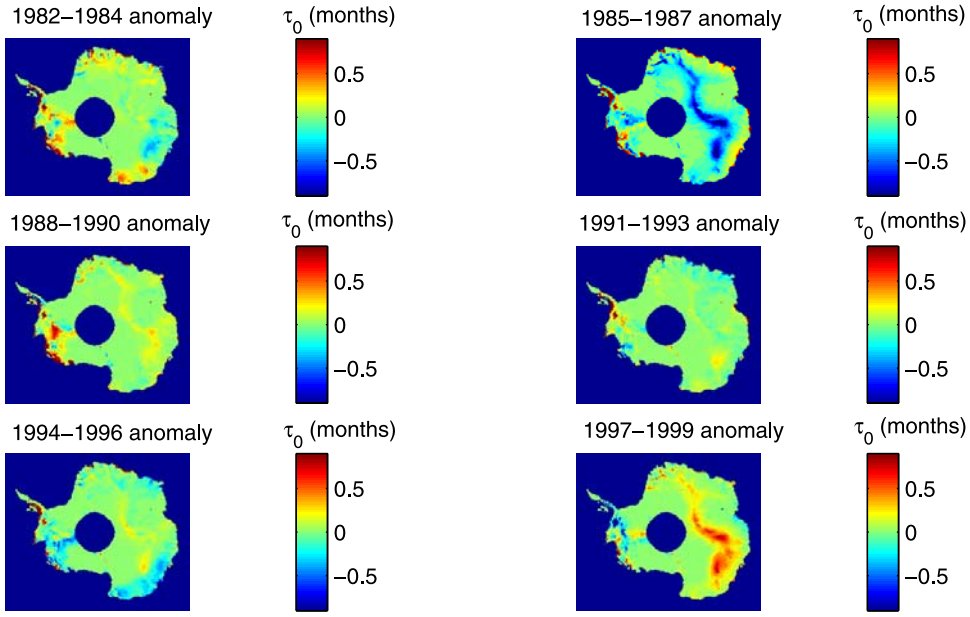

Figure 3. Temporal variability in best fit values of τ_0, as estimated from 3-year blocks of observations. The means of 3-year values of τ_0 agree with τ_0 values inferred from the full 18-year data set taken as a whole.

all pixels north of 85°S (the limit of SMMR coverage), using the AVHRR surface temperature data to simulate microwave data that were compared to the SMMR/SSM/I 37 V microwave data, from 1982 to 1999, with those pixels removed where surface melting may be significant [*Schneider and Steig*, 2002; *Schneider et al.*, 2004]. To examine temporal variability, the 37 V τ_0 was calculated from the AVHRR time series broken into six 3-year sections. Figure 3 shows the six anomaly maps produced by subtracting each 3-year τ_0 estimate from the 1982–1999 τ_0 estimate. We note that the mean of the six 3-year τ_0 is nearly identical to the 18-year (1982–1999) τ_0 at all pixels across Antarctica. The precision of the τ_0 estimates is thus fairly insensitive to the length of the record used to calculate it.

[19] Over the whole of Antarctica, no single relationship between τ_0 and accumulation would be expected from the results in Figure 2; rather, the spatial pattern of τ_0 correlates with ice divides and perhaps other topographic features. Still, for a large region near Byrd Station in West Antarctica, a strong relationship is evident. A subsection of the 37 V τ_0 map near Byrd Station, extending to both sides of the main West Antarctic ice divide, was extracted to compare with radar-generated accumulation rates (Figure 4) and U.S. ITASE ice core accumulation rates (Figure 5). The results show a strong linear relationship between τ_0 and accumulation rate (Figure 6) for both the radar data and the ice core data, up to accumulation rates of about 50 cm/yr ice equivalent. Three of the ITASE cores, located toward the Antarctic Peninsula and having generally higher accumulation rates, appear as outliers. The outliers are not entirely surprising because of the differences in climate between the West Antarctic divide and three ice core sites. The different regional climates produce different firn structures and fabrics that correspond to changes in microwave extinction length and thermal diffusivity, suggesting the possibility of different relationships between τ_0 and accumulation of different snow facies. Nevertheless, the linear correlation for the rest of the data suggests that τ_0 could be used to estimate accumulation rates in specific geographic areas.

[20] The observed correlation between τ_0 and accumulation rate near Byrd could be driven by changes in thermal diffusivity, in extinction length, or in both, as described in section 2. Without additional field measurements of extinction length over the region we cannot distinguish whether changes in thermal diffusivity or extinction length dominate changes in τ_0. We can, however, use independently modeled extinction length and existing field thermal conductivity measurements to determine whether variations in τ_0 are consistent with existing data and theory.

5. Sensitivity Analysis

[21] A few field measurements of thermal diffusivity provide an independent check on our calculations of τ_0. *Courville et al.* [2007] obtained thermal conductivity and density measurements at two sites in East Antarctica, one with "high" accumulation (4.29 cm/yr ice equivalent) and the second with "low" accumulation site (3.22 cm/yr ice equivalent). The thermal conductivity and density data at each site were used to calculate the thermal diffusivity. At these two sites the thermal diffusivity decreased from the low-accumulation site to the high-accumulation site, consistent with the observed relationship between accumulation and τ_0. Given the field thermal diffusivity measurements and τ_0, equation (5) was used to determine the expected extinction lengths at 37 GHz of 0.27 ± 0.03 cm and 0.31 ± 0.03 m for the low- and high-accumulation sites, respectively. These results are very similar to *Surdyk*'s [2002] modeled extinction lengths of 0.2–0.3 m at 37 GHz for

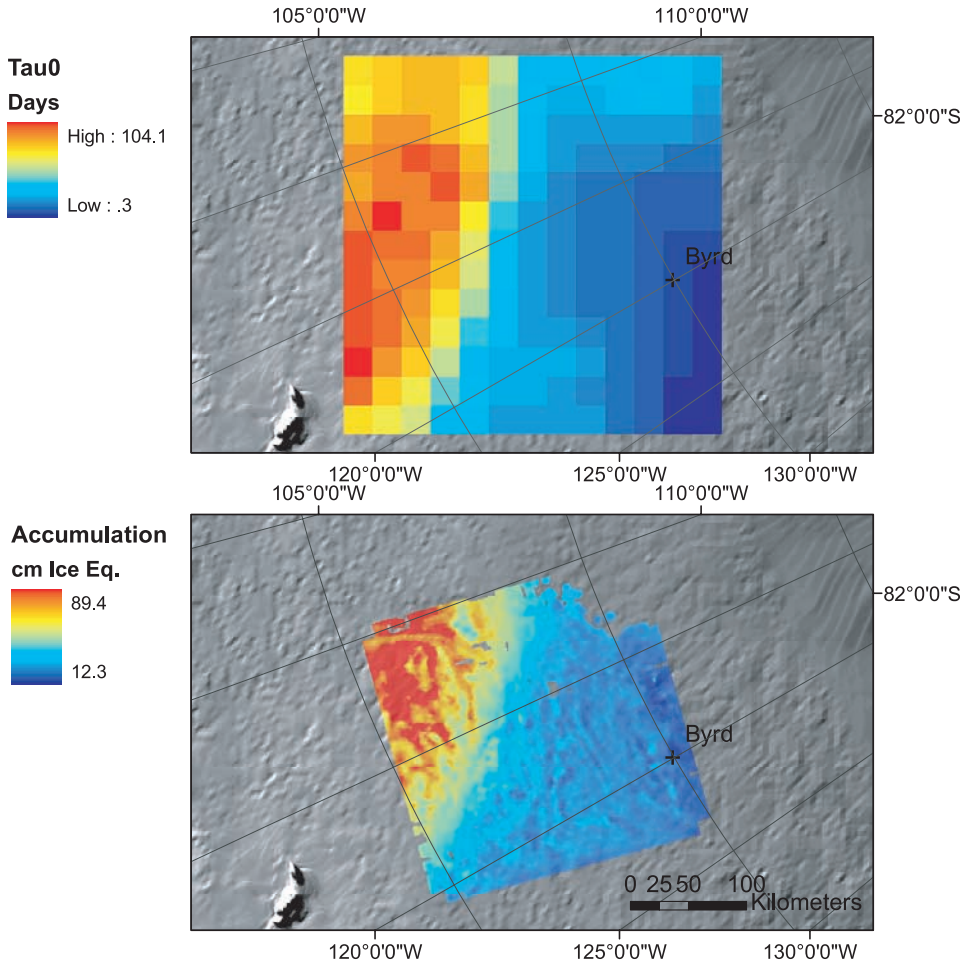

Figure 4. (top) Map of the extinction-diffusion timescale, τ_0, near Byrd Station. (bottom) Map of millennial timescale accumulation rate near Byrd Station [*Morse et al.*, 2002] derived from depth variations of ice core dated layers observed in airborne ice-penetrating radar data.

similar firn conditions, suggesting that τ_0 can be used to determine extinction lengths.

[22] Clearly, the relationship between τ_0 and accumulation is more complicated than the linear relationship near Byrd Station. Preliminary investigation of accumulation rates in East Antarctica suggests that for the very lowest accumulation rates the τ_0-accumulation relationship is more highly scattered than observed in our West Antarctic test region. We note, though, that accumulation data for East Antarctica are often sparser and very difficult to measure. The linear relationship also appears to fail for the highest accumulation rates, as observed in the outlier cores noted in Figure 5 and the increased scatter in the data in Figure 6 at accumulation rates greater than 50 cm/yr ice equivalent. It is likely that when accumulation rates cross this threshold, the extinction length is shallow compared to the annual accumulation, and snow properties become increasingly independent of accumulation rate.

[23] Finally, it is interesting to consider whether the temporal changes in τ_0, apparent in Figure 3, might be used to estimate temporal accumulation rate changes for those areas where the linear relationship appears to hold. While the strong variability observed in East Antarctica is not readily explained in terms of accumulation rate, the variations observed in West Antarctica are at least suggestive of the observed accumulation rate variability. Notably, the largest recent El Niño events occurred in 1982–1983 and 1997–1998, corresponding to the 3-year period with the greatest positive and negative τ_0 anomalies in West Antarctica. *Bromwich and Rogers* [2001] have noted previously that the West Antarctic accumulation rate response to El Niño in these years was of opposite sign.

6. Conclusions

[24] This work relates surface temperature to satellite brightness temperature through a convolution equation dependent on a characteristic timescale, the extinction-diffusion time, τ_0. This relationship describes how surface temperature changes that occurred in the past, still recorded in the firn, influence current brightness temperatures. Here τ_0 is dependent upon firn microstructure controlling the microwave extinction length and thermal conductivity.

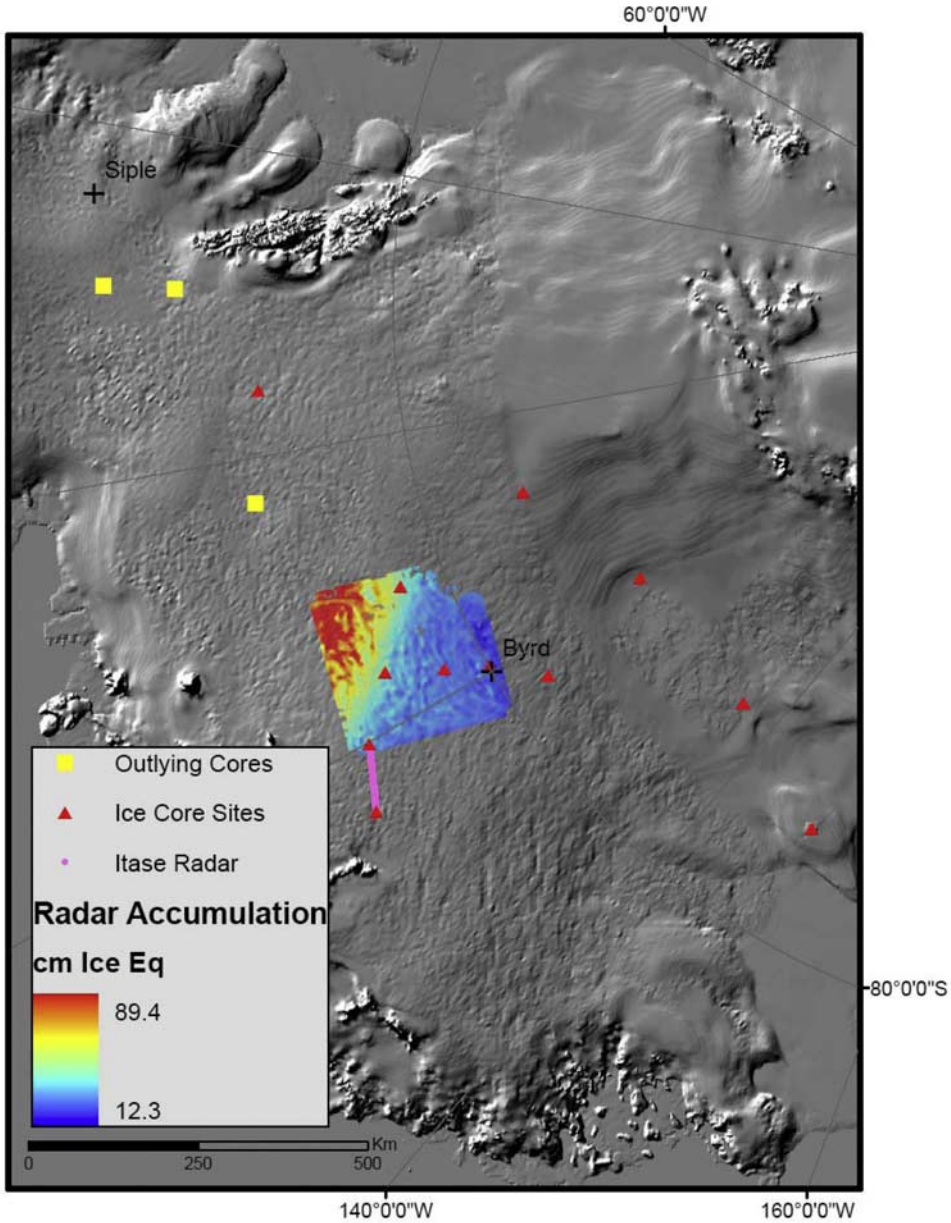

Figure 5. Locations of ice core derived and radar-derived accumulation rate data. Ice core derived accumulation data are averages over periods of decades to centuries. Cores with data that agree with the accumulation rate/τ_0 relationship derived from radar data are shown in red, whereas cores which disagree are shown in yellow.

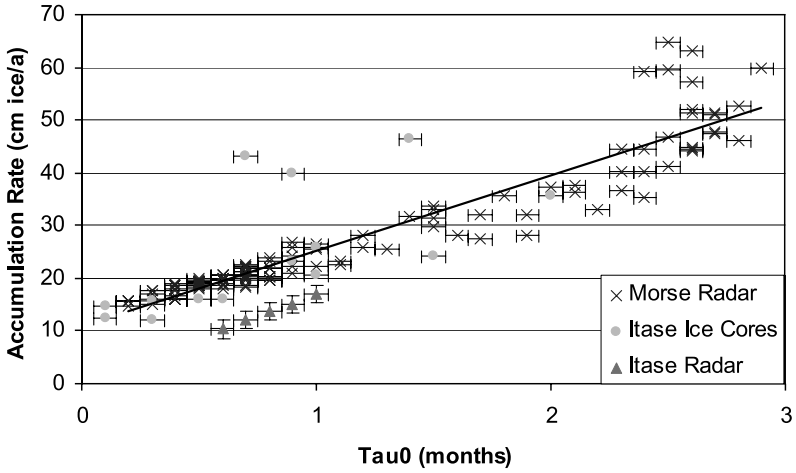

Figure 6. Observed correlation between accumulation rates derived from radar layers and ice cores and the extinction-diffusion time, τ_0, for the region near Byrd Station, extending across the West Antarctic Divide. The U.S. International Trans-Antarctic Scientific Expedition (ITASE) radar line, which appears slightly lower than the other data, is probably explained by the temporal difference in the averages. The Morse radar is averaged over the past 2500 years, while the ITASE radar is averaged over the past 34 years.

[25] The extinction-diffusion time varies in space and time over Antarctica. Near Byrd Station, Antarctica, where excellent ground-based accumulation rate data exist, τ_0 is linearly related to accumulation over a broad range from approximately 10 to 50 cm/yr ice equivalent. In East Antarctica, τ_0 is not simply related to accumulation rate, suggesting a more complex relationship between firn properties and accumulation rate, which deserves further investigation. Nevertheless, these results suggest the extinction-diffusion time may be useful for deriving accumulation rate over specific large geographic regions on polar ice sheets.

[26] **Acknowledgments.** We would like to thank the NASA Jenkins Predoctoral Fellowship Program and the National Science Foundation (grants OPP 0126161 and OPP 0440414) for supporting this research. V. P. Suchdeo, NASA Goddard Space Flight Center Cryospheric Sciences Branch, Sigma Space, enabled access to passive microwave and automatic weather station data.

References

Bindschadler, R. (1998), Monitoring ice sheet behavior from space, *Rev. Geophys.*, *36*, 79–104.

Bromwich, D. H., and A. N. Rogers (2001), The El Nino–Southern Oscillation modulation of West Antarctic precipitation, in *The West Antarctic Ice Sheet: Behavior and Environment*, *Antarct. Res. Ser.*, vol. 77, edited by R. B. Alley and R. A. Bindschadler, pp. 91–103, AGU, Washington, D. C.

Comiso, J. C. (2000), Variability and trends in Antarctic surface temperatures from in situ and satellite infrared measurements, *J. Clim.*, *13*, 1674–1696.

Courville, Z. R., M. R. Albert, M. A. Fahnestock, L. M. Cathles IV, and C. A. Shuman (2007), Impacts of an accumulation hiatus on the physical properties of firn at a low-accumulation polar site, *J. Geophys. Res.*, *112*, F02030, doi:10.1029/2005JF000429.

Gloerson, P., D. Cavalieri, W. J. Campbell, and J. Zwally (1990), Nimbus-7 SMMR Polar Radiances and Arctic and Antarctic Sea Ice Concentrations, http://nsidc.org/data/nsidc-0007.html, Natl. Snow and Ice Data Cent., Boulder, Colo.

Hall, D. (1987), Influence of depth hoar on microwave emission from snow in northern Alaska, *Cold Reg. Sci. Technol.*, *13*, 225–231.

Hall, D., and J. Martinec (1985), *Remote Sensing of Ice and Snow*, 189 pp., Chapman and Hall, London.

Hollinger, J. P., J. L. Peirce, and G. A. Poe (1990), SSM/I instrument evaluation, *IEEE Trans. Geosci. Remote Sens.*, *28*, 781–790.

Kaspari, S., P. A. Mayewski, D. A. Dixon, V. B. Spikes, S. B. Sneed, M. J. Handley, and G. S. Hamilton (2005), Climate variability in West Antarctica derived from annual accumulation rate records from ITASE firn/ice cores, *Ann. Glaciol.*, *39*, 545–594.

Maslanik, J., and J. Stroeve (1990), DMSP SSM/I Daily Polar Gridded Brightness Temperatures, http://nsidc.org/data/nsidc-0001.html, Natl. Snow and Ice Data Cent., Boulder, Colo. (Updated 2007.)

Matzler, C. (1987), Applications of the interaction of microwaves with the natural snow cover, *Remote Sens. Rev.*, *2*, 259–387.

Morse, D. L., D. D. Blankenship, E. D. Waddington, and T. A. Neumann (2002), A site for deep ice coring in West Antarctica: Results from aerogeophysical surveys and thermo-kinematic modeling, *Ann. Glaciol.*, *35*, 36–44.

Paterson, W. S. B. (1994), *The Physics of Glaciers*, 3rd ed., 481 pp., Butterworth-Heinemann, Oxford, U. K.

Schneider, D. P., and E. J. Steig (2002), Spatial and temporal variability of Antarctic ice sheet microwave brightness temperatures, *Geophys. Res. Lett.*, *29*(20), 1964, doi:10.1029/2002GL015490.

Schneider, D. P., E. J. Steig, and J. C. Comiso (2004), Recent climate variability in Antarctica from satellite-derived temperature data, *J. Clim.*, *17*, 1569–1583.

Shuman, C. A., and J. C. Comiso (2002), In situ and satellite surface temperature records in Antarctica, *Ann. Glaciol.*, *34*, 106–112.

Shuman, C. A., and C. R. Stearns (2001), Decadal-length composite inland West Antarctic temperature records, *J. Clim.*, *14*(9), 1977–1988.

Shuman, C. A., R. B. Alley, S. Anandakrishnan, and C. R. Stearns (1995), An empirical technique for estimating near-surface air temperature trends in central Greenland from SSM/I brightness temperatures, *Remote Sens. Environ.*, *51*, 245–252.

Shuman, C. A., H. J. Zwally, B. E. Schutz, A. C. Brenner, J. P. DiMarzio, V. P. Suchdeo, and H. A. Fricker (2006), ICESat Antarctic elevation data: Preliminary precision and accuracy assessment, *Geophys. Res. Lett.*, *33*, L07501, doi:10.1029/2005GL025227.

Spikes, V. B., G. S. Hamilton, S. A. Arcone, S. Kaspari, and P. A. Mayewski (2004), Variability in accumulation rates from GPR profiling on the West Antarctic plateau, *Ann. Glaciol.*, *39*, 238–244.

Surdyk, S. (2002), Using microwave brightness temperature to detect short-term surface air temperature changes in Antarctica: An analytical approach, *Remote Sens. Environ.*, *80*, 256–271.

Vaughan, D. G., J. L. Bamber, M. Giovinetto, J. Russell, and A. P. R. Cooper (1999), Reassessment of net surface mass balance in Antarctica, *J. Clim.*, *12*, 933–946.

Winebrenner, D. P., R. J. Arthern, and C. A. Shuman (2001), Mapping Greenland accumulation rates using observations of thermal emission at 4.5-cm wavelength, *J. Geophys. Res.*, *106*, 33,919–33,934.

Winebrenner, D. P., E. J. Steig, and D. P. Schneider (2004), Temporal co-variation of surface and microwave brightness temperatures in Antarctica, with implications for the observation of surface-temperature variability using satellite data, *Ann. Glaciol.*, *39*, 346–350.

Zwally, H. J. (1977), Microwave emissivity and accumulation rate of polar firn, *J. Glaciol.*, *18*, 195–215.

Zwally, H. J., and M. B. Giovinetto (1995), Accumulation in Antarctica and Greenland derived from passive-microwave data: A comparison with contoured compilations, *Ann. Glaciol.*, *21*, 123–130.

L. S. Koenig, E. J. Steig, and D. P. Winebrenner, Department of Earth and Space Sciences, University of Washington, 70 Johnson Hall, Campus Box 351310, Seattle, WA 98185-1310, USA. (lorak@u.washington.edu; steig@u.washington.edu; dpw@apl.washington.edu)

C. A. Shuman, Cryospheric Sciences Branch, NASA Goddard Space Flight Center, Code 971, Greenbelt, MD 20771, USA. (christopher.a.shuman@nasa.gov)